

Direct evidence of ferromagnetism in a quantum anomalous Hall system

Wenbo Wang,¹ Yunbo Ou,² Chang Liu,² Yayu Wang,^{2,3} Ke He,^{2,3} Qi-kun Xue,^{2,3} and Weida Wu^{1, a)}

¹⁾*Department of Physics and Astronomy, Rutgers University, Piscataway, New Jersey 08854, USA*

²⁾*State Key Laboratory of Low Dimensional Quantum Physics, Department of Physics, Tsinghua University, Beijing 100084, China*

³⁾*Collaborative Innovation Center of Quantum Matter, Beijing 100084, P. R. China*

(Dated: 5 February 2022)

The quantum anomalous Hall (QAH) systems are of great fundamental interest and of potential application because of dissipationless conduction without external magnetic field¹⁻⁹. The QAH effect has been realized in magnetically doped topological insulator thin films¹⁰⁻¹⁴. However, full quantization requires extremely low temperature ($T < 50$ mK) in the initial works, though it was significantly improved with modulation doping or co-doping of magnetic elements^{15,16}. Improved ferromagnetism was indicated in these thin films, yet a direct evidence of long-range ferromagnetic order is lacking. Herein, we present direct visualization of long-range ferromagnetic order in thin films of Cr and V co-doped (Bi,Sb)₂Te₃ using low-temperature magnetic force microscopy with *in-situ* transport. The magnetization reversal process reveals a typical ferromagnetic domain behavior, *i.e.*, domain nucleation and domain wall propagation, in contrast to much weaker magnetic signals observed in the end members, possibly due to superparamagnetic behavior¹⁷⁻¹⁹. The gate dependence of magnetic reversal indicates a significant role of bulk carrier-mediated exchange interactions. The observed long-range ferromagnetic order resolves one of the major challenges in QAH systems, and paves the way to high-temperature dissipationless conduction by exploring magnetic topological insulators.

^{a)}Corresponding author: wdwu@physics.rutgers.edu

Dissipationless conduction is technologically appealing because of a wide range of potential applications. There are two ways to achieve dissipationless conduction in condensed matter systems, superconductivity and topological chiral edge states. Therefore, high-temperature superconductivity, a great example of dissipationless conduction, has been extensively investigated for decades^{20–23}. Dissipationless conduction due to chiral edge states is realized in quantum Hall effect (QHE), which requires low temperature and external magnetic field. The closely related phenomenon, quantum anomalous Hall effect (QAHE) doesn't need an external magnetic field, so it attracts significant attention recently. The realization of QAHE requires time reversal symmetry breaking and topologically nontrivial band structure. There have been a few theoretical proposals^{1–9}, and eventually it is experimentally realized in magnetically doped 3D topological insulator (TI) thin films^{10–12,24}. Here the ferromagnetism was introduced by doping magnetic elements. The broken time reversal symmetry opens a mass gap at the Dirac point of the topological surface states. By tuning the Fermi level inside the mass gap, the magnetic TI thin film is equivalent to two copies of half integer QHE systems²⁵. QAHE was first observed in Cr-doped $\text{Bi}_x\text{Sb}_{2-x}\text{Te}_3$ (BST) thin films synthesized by molecular beam epitaxy (MBE)¹⁰. The quantized Hall conduction, however, was observed at ultra-low temperature (~ 30 mK). This observation is soon confirmed by other groups^{11–14}. Later, a robust QAHE with higher precision quantization was observed in the V-doped BST thin film, which is a hard ferromagnet with a larger coercive field (H_c) and higher Curie temperature (T_C) with the same doping level²⁴. Yet, ultra-low temperature ($T < 50$ mK) is still needed to achieve full quantization. Therefore, it is imperative to understand the origin of the ultra-low temperature of full quantization, which is still under debate.

Magnetic inhomogeneity has been proposed to be one of the main factors that limit the QAH temperature. The electronic inhomogeneity, disordered ferromagnetic or superparamagnetic behavior, have been reported in Cr-doped BST thin films^{17–19,26}. In these cases, the reduced QAH temperature is likely limited by the regions with the smallest exchange gap in the Cr-doped systems. While modulation doping of Cr was shown to improve the quantization temperature in penta-layer thin films¹⁵, it is unclear whether it reduces magnetic inhomogeneity. On the other hand, recent angle-resolved photoemission spectroscopy (ARPES) studies of V-doped BST thin films suggest that valance band maximum (VBM) is above the Dirac point²⁷ so that ultra-low temperature and disorders are needed to localize

the bulk carriers. The different mechanisms of reduced quantization temperature indicate that Cr and V co-doping might help to enhance the performance. Furthermore, alloy doping is commonly known as an effective route to improve ferromagnetic order in a diluted magnetic semiconductor^{28,29}.

Indeed, enhanced QAH temperature was observed in Cr and V co-doped BST thin films¹⁶. At optimal Cr/V ratio, full quantization was achieved at 300 mK, an order of magnitude higher than the end members with single dopants¹⁶. The Hall hysteresis loop is more square-like, suggesting a sharper magnetization reversal, *i.e.*, less magnetic inhomogeneity. Furthermore, the temperature dependence of anomalous Hall resistance is more mean-field-like. These observations indicate improved ferromagnetism in Cr/V co-doped TI thin films. However, the direct microscopic evidence of long-range ferromagnetic ordering is still lacking. In this letter, we reported a systematic study of Cr/V co-doped BST thin films using the magnetic force microscopy (MFM). Our MFM results reveal a clear ferromagnetic domain behavior of the magnetization reversal process in the optimally doped BST thin films, confirming the long-range ferromagnetic ordering in this QAH system. Furthermore, the ferromagnetism of co-doped thin films is robust against significant change of bulk charge carrier density, though exchange interaction is enhanced by hole doping. This indicates a significant contribution from the Ruderman-Kittel-Kasuya-Yosida (RKKY) exchange coupling^{30,31}. The direct evidence of long-range ferromagnetic order eases the concern of the fragility of QAHE due to magnetic inhomogeneity, alleviating the need of ultra-low temperature to achieve full quantization. Our results will encourage further exploration of QAHE in magnetically doped topological materials for dissipationless conduction at elevated temperature.

Figure 1(a) shows the schematic picture of the Hall bar device of the magnetic TI thin films fabricated for MFM and *in-situ* transport measurements. Three $(\text{Cr}_y\text{V}_{1-y})_{0.19}(\text{Bi}_x\text{Sb}_{1-x})_{1.81}\text{Te}_3$ films ($y = 0, 0.16, 1$, respectively and $x \sim 0.4$) are fabricated into the Hall bar devices for MFM and *in-situ* transport measurements. The $y = 0.16$ film is the optimized co-doped sample, which exhibits the best ferromagnetic behavior and the highest QAH temperature among the co-doped BST films¹⁶. The temperature dependence of the Hall resistance shows a mean-field-like behavior with the Curie temperature $T_C \approx 28$ K, indicating a robust ferromagnetism. The longitudinal resistance starts to decrease right below T_C , indicating that the sample enters the QAH regime as soon as the long-range ferromagnetic order

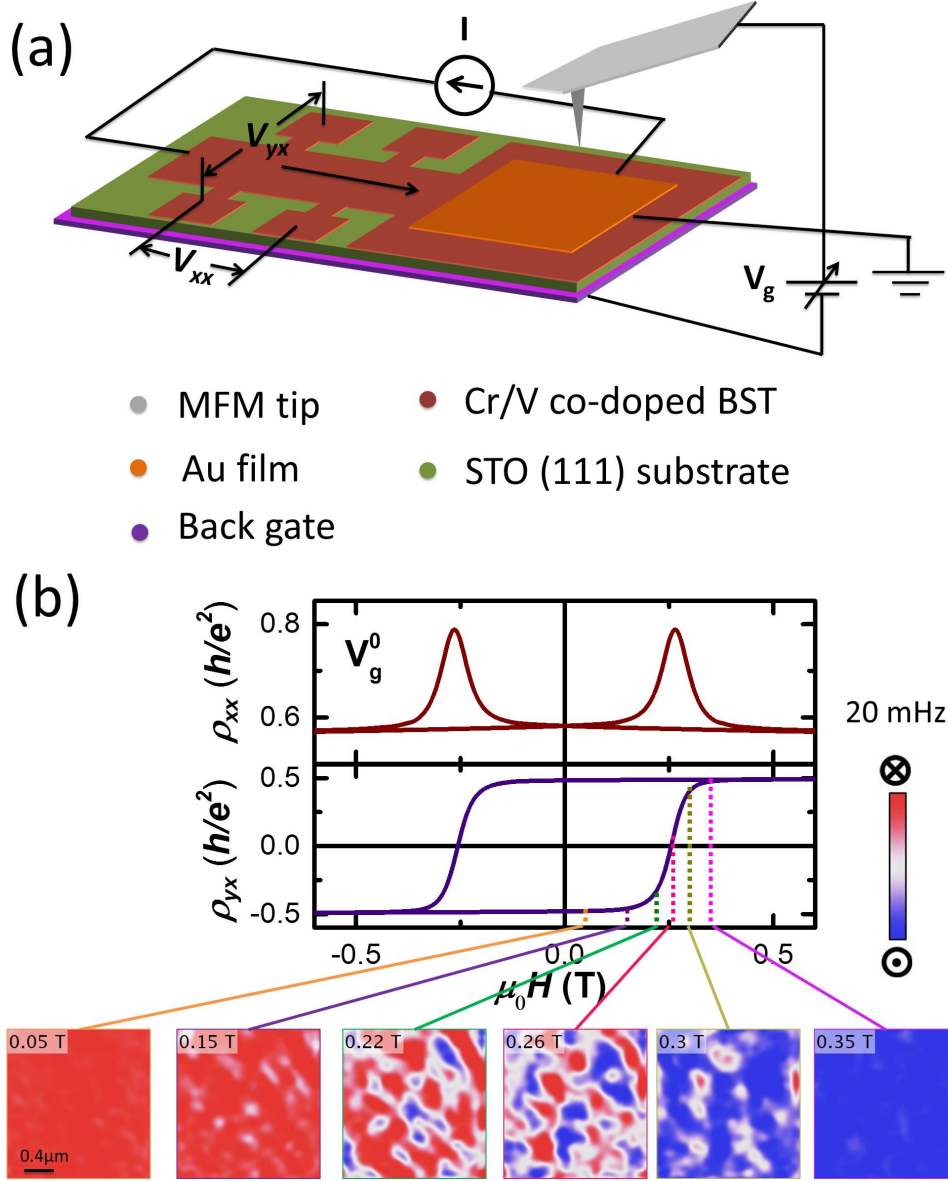


FIG. 1. **Schematic of *in-situ* transport setup and MFM data of the Cr/V co-doped BST film at 5 K** | (a) A cartoon of the Hall bar device for MFM and *in-situ* transport measurements. The 5 QL Cr/V co-doped BST thin film was grown on STO(111) substrate using MBE, followed by deposition of a layer of 15 nm Au film. Both Au film and magnetic tip were grounded to eliminate any electrostatic interaction between them. A back-gate voltage V_g was applied to the bottom electrode to tune the charge carrier density. The Hall resistance ρ_{yx} and longitudinal resistance ρ_{xx} were obtained by measuring V_{yx} and V_{xx} . (b) 5 K field-dependent MFM images and *in-situ* transport data at $V_g^0 \simeq 10$ V. The MFM images show ferromagnetic domain behavior during the magnetization reversal from 0.15 T to 0.35 T, consistent with transport data.

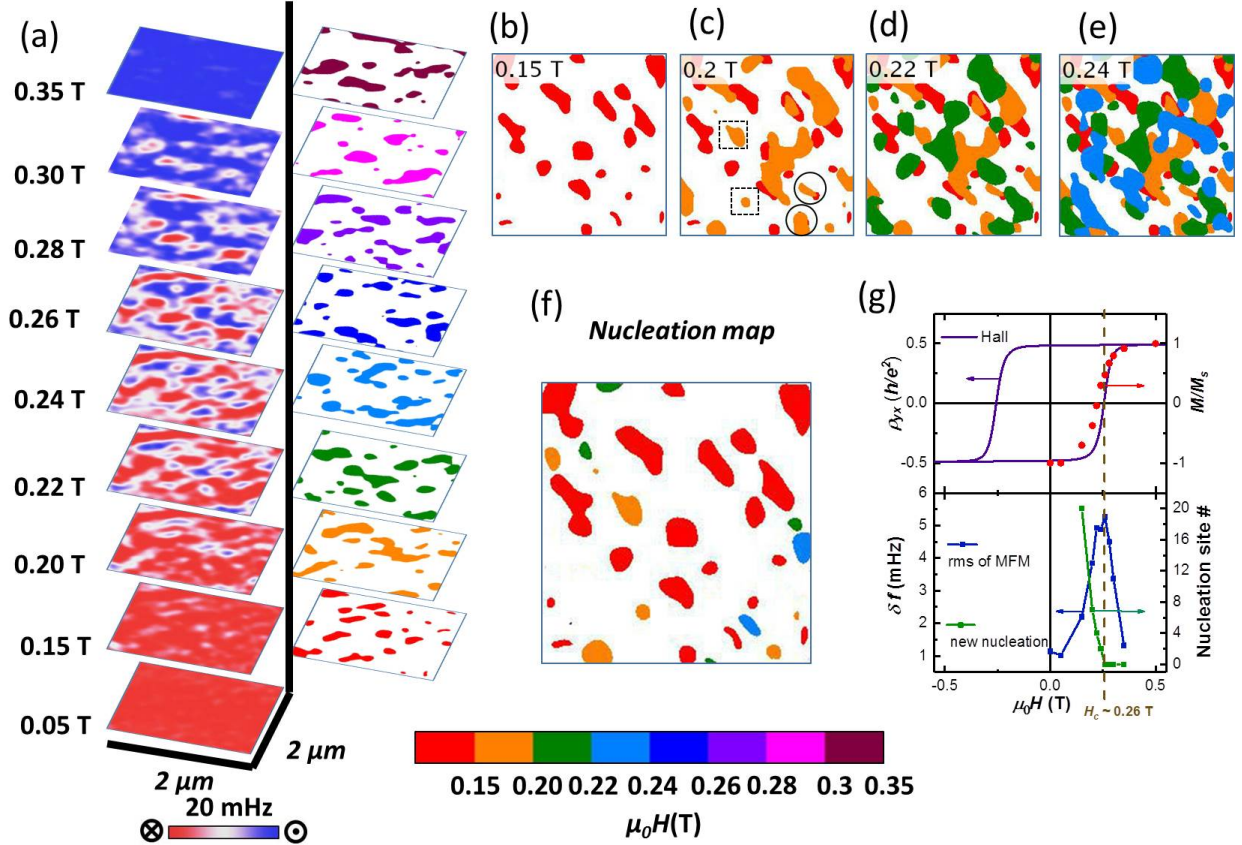


FIG. 2. **The magnetization reversal process at 5 K at neutral point V_g^0 .** | (a) Left column: a stack of MFM images from 0.05 T to 0.35 T to illustrate the domain evolution; Right column: the differential images by taking the difference between adjacent MFM images. Different colors represent local magnetization reversed at different magnetic fields. (b)-(e) Images of the reversed areas at various fields by combining the differential images, which illustrate domain nucleation and domain wall propagation. Dashed squares label the nucleation sites and solid circles label the domain wall propagation. (f) Nucleation map shows the distribution of nucleation sites appearing at various fields. (g) H -dependence of normalized magnetization M/M_s , estimated from domain population, is quantitatively consistent with the anomalous Hall loop. The domain contrast (δf_{rms}) peaks at H_c , while number of nucleation sites reduces to zero at H_c .

forms (Supplementary Fig.S1(a)). The end member ($y = 0$ or 1), however, enters the QAH regime at a much lower temperature. A gate voltage was applied to the back of STO substrate to tune the Fermi level. At 1.5 K, the Hall resistance reaches $0.95 h/e^2$ at V_g^0 (Supplementary Fig.S1). Such a quantization level was only be achieved below 50 mK in

singly Cr- or V-doped thin films^{10–12,24}. All MFM images presented here were taken at 5 K, the base temperature of our MFM system. The Hall traces at both 1.5 K and 5 K show similar square-like hysteresis loop, suggesting no qualitative difference between these two temperatures. Furthermore, a larger coercive field (H_c) with sharper reversal was observed at 1.5 K, suggesting better ferromagnetism at the lower temperature. Therefore, the observed ferromagnetic behavior is expected to persist at the lower temperature where full quantization was observed on the same sample¹⁶.

Fig. 1(b) shows the MFM images and *in-situ* transport data (ρ_{xx} and ρ_{yx}) of optimally doped film at $V_g^0 \simeq 10$ V at various magnetic fields. The $\rho_{yx}(H)$ loop shows a saturation $\sim 0.5 h/e^2$ with a coercive field $H_c \sim 0.26$ T. The magnetization reversal process from negatively (red) to positively (blue) magnetized state is illustrated in the MFM images at the bottom of Fig. 1(b). The negatively saturated state has very weak magnetic contrast with a small positive field (+0.05 T), indicating a single domain state persist at a small reversed field. The single domain state is static and stable during the course of MFM measurements. The observed stable single domain state is in sharp contrast to the superparamagnetic behavior previously reported in Cr-doped BST films, where significant magnetic relaxation was already observed at zero magnetic field¹⁷. At 0.15 T, up domains start to nucleate, represented by light blue regions. As the field increases further, up domains expand and down domains shrink. At coercive field H_c where $\rho_{yx} = 0$ and ρ_{xx} peaks at $\sim 0.8 h/e^2$, equally populated up and down domains were observed, confirming the zero magnetization state ($M = 0$). For $H \geq 0.35$ T, no red regions is visible in MFM image, indicating the system is in a saturated (single domain) state. The MFM observation of ferromagnetic domain behavior is in excellent agreement with the *in-situ* transport data, suggesting local observation is representative of the global (bulk) properties.

The ferromagnetic domain behavior can be further illustrated with the differential MFM images, the difference between MFM images of adjacent fields as shown in Fig. 2(a). The locations where the changes of MFM signal are above the noise level (~ 2 mHz) are defined as the newly reversed regions. They are marked by different colors at each field value, which are shown in the right column of Fig. 2(a). Here the unchanged areas are marked with white color. In Figs. 2(b)-(e), these differential images were stacked together to show the spatial correlations of magnetization reversal events to differentiate domain nucleation from domain expansion. (See supplementary information Fig. S4 for complete data set) For example, as

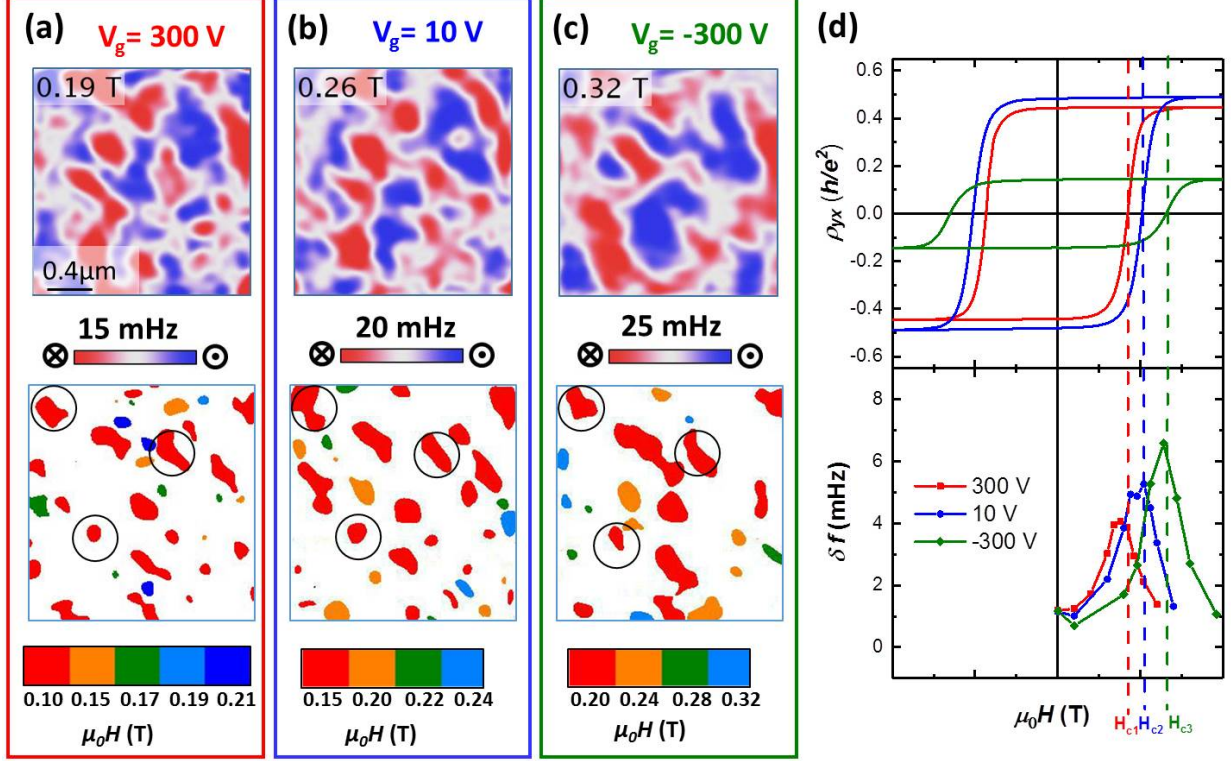


FIG. 3. **Gate dependence of ferromagnetic behavior.** | (a)-(c) MFM images around coercive field and nucleation-site maps, respectively at $V_g = 300$ V, 10 V and -300 V. Larger domain size and stronger domain contrast were observed in the $V_g = -300$ V (hole-doping). Black circles label some of the common nucleation sites at three different V_g values. (d) The Hall resistance (top panel), MFM domain contrasts (δf_{rms}) (bottom panel) as a function of magnetic fields at three different V_g values. The H_c deduced from two panels are consistent with each other, as $H_{c1} \approx 0.21$ T ($V_g = 300$ V), $H_{c2} \approx 0.26$ T ($V_g^0 = 10$ V), $H_{c3} \approx 0.33$ T ($V_g = -300$ V).

shown in Fig. 2(c), some of the newly reversed regions (yellow) at 0.2 T have no correlations with previously reversed regions (red). These regions, labeled by dashed squares, are new nucleation sites. The other yellow regions, labeled by solid circles, have clear overlap with the red regions, demonstrating domain growth due to domain wall propagation. All nucleation sites during the reversal process are summarized in Fig. 2(f). As summarized in Fig. 2(g), the number of nucleation sites decreases with increasing H , and drops to zero for $H > H_c$, indicating a crossover from domain nucleation to domain wall propagation.

In addition to direct visualization of ferromagnetic domain behavior, MFM data can also be used to extract the hysteresis loop of normalized magnetization (M/M_s), which is

estimated from the populations of up and down domains³². As shown in Fig.2(k), the $M/M_s(H)$ curve quantitatively agrees with $\rho_{yx}(H)$ loop, confirming conventional scaling behavior of anomalous Hall effect: $\rho_{yx} \propto M$. The agreement between local (M) and global (ρ_{yx}) measurements demonstrate that our MFM results are representative of the bulk magnetic properties. Consistently, the domain contrast, estimated with the root-mean-square (RMS) value of MFM signal (δf_{rms}), peaks at H_c when up and down domains are equally populated. The observed domain behavior provides unambiguous evidence of long-range ferromagnetic order in the optimally Cr/V co-doped BST thin films. In contrast, MFM measurements on singly doped BST films do not reveal clear ferromagnetic behavior. (See supplementary information for MFM results of end members) Therefore, our MFM data provide direct evidence that long-range ferromagnetic order is essential for the enhancement of QAH temperature¹⁶.

The long-range ferromagnetic order is one of key ingredients of QAHE. Yu *et al.* proposes van Vleck mechanism in magnetically doped TIs, which gains some experimental support^{5,33}. However, other studies indicate that RKKY type exchange mechanism plays a significant role^{34,35}. To shed light on the exchange mechanisms, we investigate the bulk carriers dependence of the ferromagnetism by applying gate voltage (V_g). Similar to the neutral point V_g^0 case, both electron-doped (300 V) and hole-doped (-300 V) states show typical ferromagnetic domain behavior, confirming that long range ferromagnetic order is robust against tuning of Fermi level near neutral point (see Supplementary Information Fig.S5 and Fig.S6). Fig.3(a)-(c) show the MFM images at H_c and the nucleation maps of the three gate voltages. Comparing the three multi-domains states, the hole-doping results in larger domain size, fewer nucleation sites, and stronger domain contrast, while electron doping results in opposite trend. Consistently, H_c is enhanced (suppressed) by hole (electron) doping, as shown in the $\rho_{yx}(H)$ loops in Fig.3(d). On the other hand, both hole and electron doping away from neutral point suppresses anomalous Hall effect. Note that domain contrast of multi-domain state is proportional to saturated magnetization³⁶. The enhanced domain contrast at H_c indicate an increase of saturated magnetization with hole doping. Comparing to the local magnetic moment density, the gate-induced charge carrier density is negligible. (See supplementary information for estimation of induced charge carrier density) So the saturated magnetization at zero temperature $M_s(0)$ is unlikely to change within our gating capability. Therefore, the enhancement of the magnetization at 5 K indi-

cates a decrease of reduced temperature T/T_C , *i.e.*, *i.e.*, higher T_C due to an enhancement of exchange coupling in the hole-doped films. This is consistent with higher H_c and fewer nucleation sites in the hole-doped state. In principle, the Dirac surface state carriers can mediate an RKKY-type exchange interaction³⁷. This mechanism is likely irrelevant in our samples because the ferromagnetism gets weaker on the electron-doping side. Interestingly some nucleation sites (labeled by black circles) are independent of gate voltages, so they are likely caused by neutral defects or imperfections that are insensitive to charge carriers. On the other hand, there are nucleation sites that do depend on gate voltages, which indicates that they might be related to charged defects.

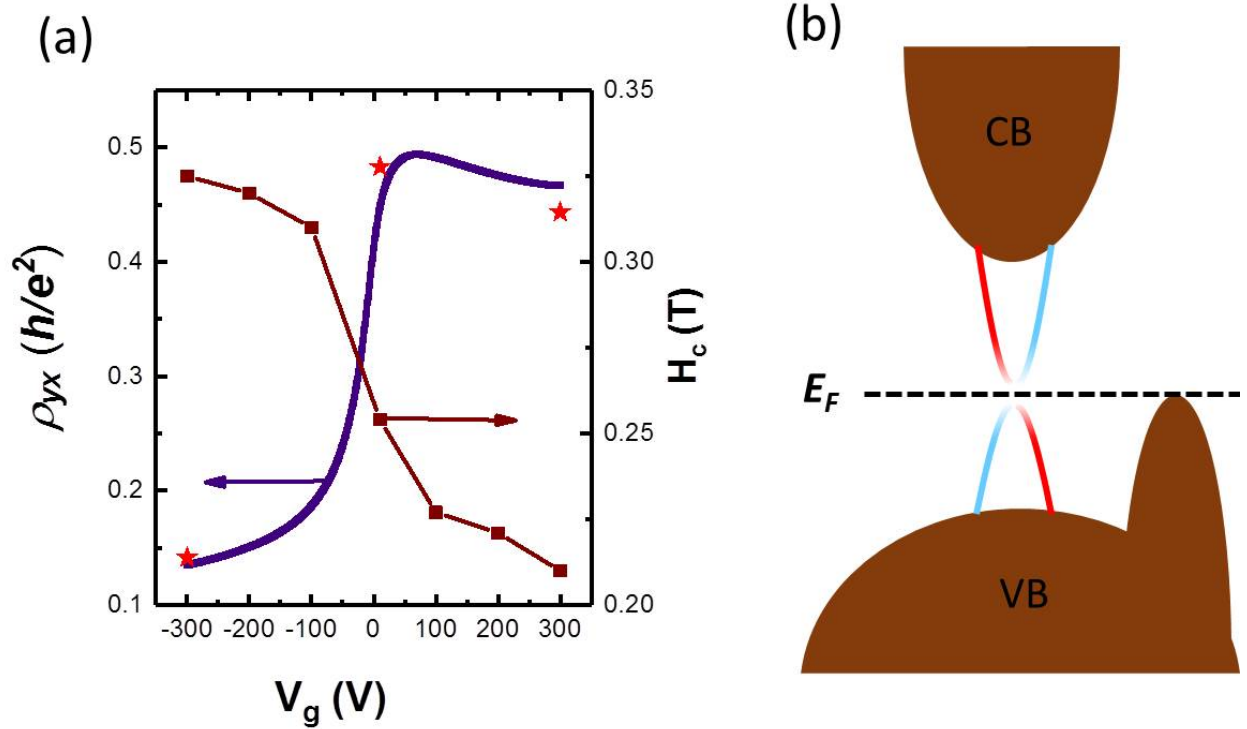


FIG. 4. **Gate dependence of the transport and magnetic properties.** | (a) ρ_{yx} and H_C vs. V_g . Red stars are the zero-field ρ_{yx} from hysteresis loops at -300 V, 10 V and 300 V. (b) The schematic picture of the band structure of the Cr/V co-doped BST film. The Dirac point of the surface state is close to VBM.

The V_g -dependence of ρ_{yx} and H_c are summarized in Fig. 4(a). The $\rho_{yx}(V_g)$ curve was measured at zero magnetic field with slowly ramping of V_g from -300 V to $+300$ V after the

film was saturated at high field. The result agrees well with the saturation state resistance from hysteresis loop measurements (red stars), indicating the film stays in the single-domain state. The $\rho_{yx}(V_g)$ shows a peak at $V_g^0 \approx 10$ V, the charge neutral point. In contrast to the non-monotonic gate dependence of ρ_{yx} , the $H_c(V_g)$ shows a monotonic behavior with significant enhancement on hole doping side, consistent with RKKY mechanism. This indicates that the VBM (or the mobility edge) is very close to the neutral (Dirac) point as shown in Fig. 4(b)²⁴. Therefore, hole-doping will introduce substantial amount of bulk charge carriers, which will favor RKKY type exchange mechanism but significantly enhance dissipation. On the other hand, electron-doping push the Fermi level up above the VBM, but presumably not enough to reach the conduction band minimum (CBM). Therefore, electron-doping likely only introduce small amounts of surface state electrons, which slightly enhance dissipation. Previous ARPES results of V-doped BST film suggest that the Dirac point is below the VBM²⁷. Thus doping a small amount of Cr into V-doped BST film might slightly lower the VBM. Alternatively, Cr/V co-doping effectively enhance scattering of bulk carriers, promoting localization without reducing the mass gap.

In conclusion, we present a systematic MFM with *in-situ* transport study of the ferromagnetic domain behavior of Cr/V co-doped BST thin films, which can achieve full quantization of Hall resistance at 300 mT. MFM results reveal clear domain nucleation and domain wall propagation during the magnetization reversal. Our results provide unambiguous evidence of the long-range ferromagnetic order in magnetic TI thin films. The gate voltage dependence of the ferromagnetism suggests that significant RKKY contribution due to bulk carriers. The observed robust ferromagnetism resolves one of the major concern in magnetically doped topological insulators, opens a door to explore high-temperature dissipationless conduction with magnetic topological materials.

METHODS

A. Sample preparation

Epitaxial thin film Cr/V co-doped BST films capped with 2 nm Al was grown on heat treated SrTiO₃(111) substrate by co-evaporation in a molecular beam epitaxy (MBE) system. The nominal thickness of the film is 5 quintuple layers (QL). The film was scratched by

hand into a Hall bar shape connected with a large square-like area for MFM measurements. A layer of ~ 15 nm Au film was deposited on the square area to eliminate electrostatic interaction between the sample and magnetic tip.

B. MFM measurement

The MFM experiments were carried out in a homemade cryogenic atomic force microscope (AFM) using commercial piezoresistive cantilevers (spring constant $k \approx 3$ N/m, resonant frequency $f_0 \approx 42$ kHz). The homemade AFM is interfaced with a Nanonis SPM Controller (SPECS) and a commercial phase-lock loop (SPECS)^{32,38}. MFM tips were prepared by depositing nominally 100 nm Co film onto bare tips using e-beam evaporation. MFM images were taken in a constant mode with the scanning plane ~ 40 nm above the sample surface. To avoid the relaxation effect (domain wall creeping) near H_c and to minimize the stray field effect of the MFM tip, all MFM images were taken at low magnetic field ~ 0.05 T after the magnetic field was ramped to the desired values. The MFM signal, the change of cantilever resonant frequency, is proportional to out-of-plane stray field gradient³⁹. Electrostatic interaction was minimized by nulling the tip-surface contact potential difference. Blue (red) regions in MFM images represent up (down) ferromagnetic domains, where magnetizations are parallel(anti-parallel) with the positive external field.

C. *in-situ* transport measurement

The magnetic TI films were fabricated into Hall bar devices. The Hall resistance and longitudinal resistance were measured by standard lock-in technique with ac current of $5 \mu\text{A}$ modulated at 314 Hz.

AUTHOR CONTRIBUTION

WWu, KH and YW conceived the project. WWu and WWa designed the MFM experiment. WWa performed MFM with *in-situ* transport measurements, and analyzed the data. YO synthesized the MBE films under the supervision of KH and QX. CL and YW carried out transport characterization of the films. WWu and WWa wrote the manuscript with inputs from all authors.

ACKNOWLEDGMENTS

We thank C. Chang for helpful discussion. This work at Rutgers is supported by the Office of Basic Energy Sciences, Division of Materials Sciences and Engineering, U.S. Department of Energy under Award number DE-SC0008147 and DE-SC0018153. The work at Tsinghua University is supported by National Natural Science Foundation of China and the Ministry of Science and Technology of China.

REFERENCES

- ¹Haldane, F. D. M. Model for a quantum Hall effect without landau levels: condensed-matter realization of the “parity anomaly”. *Phys. Rev. Lett.* **61**, 2015–2018 (1988).
- ²Onoda, M. & Nagaosa, N. Quantized anomalous Hall effect in two-dimensional ferromagnets: Quantum Hall effect in metals. *Phys. Rev. Lett.* **90**, 206601 (2003).
- ³Liu, C. X., Qi, X. L., Dai, X., Fang, Z. & Zhang, S. C. Quantum anomalous Hall effect in $\text{Hg}_{1-y}\text{Mn}_y\text{Te}$ quantum wells. *Phys. Rev. Lett.* **101**, 146802 (2008).
- ⁴Qi, X. L., Hughes, T. L. & Zhang, S. C. Topological field theory of time-reversal invariant insulators. *Phys. Rev. B* **78**, 195424 (2008).
- ⁵Yu, R. *et al.* Quantized anomalous Hall effect in magnetic topological insulators. *Science* **329**, 61–64 (2010).
- ⁶Qiao, Z. H. *et al.* Quantum anomalous Hall effect in graphene from Rashba and exchange effects. *Phys. Rev. B* **82**, 161414 (2010).
- ⁷Nomura, K. & Nagaosa, N. Surface-quantized anomalous Hall current and the magnetoelectric effect in magnetically disordered topological insulators. *Phys. Rev. Lett.* **106**, 166802 (2011).
- ⁸Zhang, H., Lazo, C., Bluegel, S., Heinze, S. & Mokrousov, Y. Electrically tunable quantum anomalous hall effect in graphene decorated by 5d transition-metal adatoms. *Phys. Rev. Lett.* **108**, 056802 (2012).
- ⁹Ezawa, M. Valley-polarized metals and quantum anomalous Hall effect in silicene. *Phys. Rev. Lett.* **109**, 055502 (2012).
- ¹⁰Chang, C.-Z. *et al.* Experimental observation of the quantum anomalous Hall effect in a magnetic topological insulator. *Science* **340**, 167–170 (2013).

- ¹¹Checkelsky, J. G. *et al.* Trajectory of the anomalous Hall effect towards the quantized state in a ferromagnetic topological insulator. *Nat. Phys.* **10**, 731 (2014).
- ¹²Kou, X. *et al.* Scale-invariant quantum anomalous Hall effect in magnetic topological insulators beyond the two-dimensional limit. *Phys. Rev. Lett.* **113**, 137201 (2014).
- ¹³Kou, X. *et al.* Metal-to-insulator switching in quantum anomalous Hall states. *Nat. Comm.* **6**, 8474 (2015).
- ¹⁴Feng, Y. *et al.* Observation of the zero Hall plateau in a quantum anomalous Hall insulator. *Phys. Rev. Lett.* **115**, 126801 (2015).
- ¹⁵Mogi, M. *et al.* Magnetic modulation doping in topological insulators toward higher-temperature quantum anomalous Hall effect. *Appl. Phys. Lett.* **107**, 182401 (2015).
- ¹⁶Ou, Y. *et al.* Enhancing the quantum anomalous hall effect by magnetic co-doping in a topological insulator (2017). Submitted.
- ¹⁷Lachman, E. O. *et al.* Visualization of superparamagnetic dynamics in magnetic topological insulators. *Sci. Adv.* **1**, e1500740 (2015).
- ¹⁸Grauer, S. *et al.* Coincidence of superparamagnetism and perfect quantization in the quantum anomalous Hall state. *Phys. Rev. B* **92**, 201304 (2015).
- ¹⁹Lee, I. *et al.* Imaging Dirac-mass disorder from magnetic dopant atoms in the ferromagnetic topological insulator $\text{Cr}_x(\text{Bi}_{0.1}\text{Sb}_{0.9})_{2-x}\text{Te}_3$. *Proc. Natl. Acad. Sci. U. S. A.* **112**, 1316–1321 (2015).
- ²⁰Bednorz, J. G. & Muller, K. A. Possible high T_c superconductivity in the Ba-La-Cu-O system. *Z. Fur Physik B-condensed Matter* **64**, 189–193 (1986).
- ²¹Wu, M. K. *et al.* Superconductivity at 93 K in a new mixed-phase Y-Ba-Cu-O compound system at ambient pressure. *Phys. Rev. Lett.* **58**, 908–910 (1987).
- ²²Maeda, H., Tanaka, Y., Fukutomi, M. & Asano, T. A new high- T_c oxide superconductor without a rare earth element. *Jpn. J. Appl. Phys., Part 2* **27**, L209–L210 (1988).
- ²³Schilling, A., Cantoni, M., Guo, J. D. & Ott, H. R. Superconductivity above 130 K in the Hg-Ba-Ca-Cu-O system. *Nature* **363**, 56–58 (1993).
- ²⁴Chang, C. Z. *et al.* High-precision realization of robust quantum anomalous Hall state in a hard ferromagnetic topological insulator. *Nat. Mater.* **14**, 473–477 (2015).
- ²⁵Grauer, S. *et al.* Scaling of the quantum anomalous Hall effect as an indicator of axion electrodynamics. *Phys. Rev. Lett.* **118**, 246801 (2017).

- ²⁶Chang, C.-Z. *et al.* Chemical-potential-dependent gap opening at the dirac surface states of Bi_2Se_3 induced by aggregated substitutional Cr atoms. *Phys. Rev. Lett.* **112**, 056801 (2014).
- ²⁷Li, W. *et al.* Origin of the low critical observing temperature of the quantum anomalous Hall effect in V-doped $(\text{Bi,Sb})_2\text{Te}_3$ film. *Sci. Rep.* **6**, 32732 (2016).
- ²⁸Andriotis, A. N. & Menon, M. Defect-induced magnetism: Codoping and a prescription for enhanced magnetism. *Phys. Rev. B* **87**, 155309 (2013).
- ²⁹Qi, S. F. *et al.* High-temperature quantum anomalous Hall effect in n-p codoped topological insulators. *Phys. Rev. Lett.* **117**, 056804 (2016).
- ³⁰Ruderman, M. A. & Kittel, C. Indirect exchange coupling of nuclear magnetic moments by conduction electrons. *Phys. Rev.* **96**, 99–102 (1954).
- ³¹Kou, X. F. *et al.* Interplay between different magnetisms in Cr-doped topological insulators. *Acs Nano* **7**, 9205–9212 (2013).
- ³²Wang, W., Chang, C.-Z., Moodera, J. S. & Wu, W. Visualizing ferromagnetic domain behavior of magnetic topological insulator thin films. *npj Quantum Mater.* **1**, 16023 (2016).
- ³³Li, M. *et al.* Experimental verification of the Van Vleck nature of long-range ferromagnetic order in the vanadium-doped three-dimensional topological insulator Sb_2Te_3 . *Phys. Rev. Lett.* **114**, 146802 (2015).
- ³⁴Li, H. *et al.* Carriers dependence of the magnetic properties in magnetic topological insulator $\text{Sb}_{1.95-x}\text{Bi}_x\text{Cr}_{0.05}\text{Te}_3$. *Appl. Phys. Lett.* **101**, 072406 (2012).
- ³⁵Chang, C.-Z. *et al.* Zero-field dissipationless chiral edge transport and the nature of dissipation in the quantum anomalous hall state. *Phys. Rev. Lett.* **115**, 057206 (2015).
- ³⁶Wang, W. *et al.* Visualizing weak ferromagnetic domains in multiferroic hexagonal ferrite thin film. *Phys. Rev. B* **95**, 134443 (2017).
- ³⁷Sessi, P. *et al.* Signatures of Dirac fermion-mediated magnetic order. *Nat Commun* **5**, 5349 (2014).
- ³⁸Wang, W. *et al.* Visualizing ferromagnetic domains in magnetic topological insulators. *APL Mater.* **3**, 083301 (2015).
- ³⁹Rugar, D. *et al.* Magnetic force microscopy: General principles and application to longitudinal recording media. *J. Appl. Phys.* **68**, 1169–1183 (1990).